RODRÍGUEZ-MILLÁN, M. et al. (2016). ″Numerical analysis of the ballistic behaviour of Kevlar® composite under impact of double-nosed stepped cylindrical projectiles″. *Journal of Reinforced Plastics and Composites*. SAGE, 2016, vol. 35(2), pp. 124-137. ISSN: 0731-6844
DOI: 10.1177/0731684415608004

Proyectos RTC-2015-3887-8 y DPI2011-23191

Numerical analysis of the ballistic behaviour of Kevlar® composite under impact of double-nosed stepped cylindrical projectiles

Marcos Rodríguez Millán, Carlos E. Moreno, Miguel Marco, Carlos Santiuste and Henar Miguélez

Abstract

This paper focuses on the numerical analysis of the ballistic performance of Kevlar®-29 under impact of different double-nosed stepped cylindrical projectiles. Numerical modelling based on finite element method was carried out in order to predict the failure mode of the target as well as the ballistic limit. A detailed analysis of the ballistic limit, failure mode and deformation of the targets due to impact of double-nosed projectiles was developed, discussed and compared with those involved in penetration of single-nosed flat and conical projectiles. Significant influence of the projectile geometry was demonstrated: the lowest ballistic limit was obtained with the conical–conical nose shape projectiles.

Keywords

Aramid fibre, Kevlar, impact, double nose shape, ballistic limit

Introduction

Composites are widely used in aerospace, defence and security industries. Defence applications; such as combat helmets, personal protections and vehicles armours; require an exhaustive analysis of composite behaviour under dynamic loading in order to satisfy the safety requirements. Personal protections are usu-ally based on fibre reinforced polymer composites, mainly aramid fibres, being Kevlar^{Õ} the most used fibre. Main advantage of this type of composites relies on their high specific sti•ness and elevated energy absorption capacity. Lightness of this family of com-posites made it suitable for personal protections with better specific properties than those obtained with unre-inforced polymers or conventional metals.

Different authors have focused attention on proper-ties and dynamic response of aramid composites (see, for instance, Refs. 1–5). Their excellent mechan-ical properties are related to their microstructure char-acterized by several features such as fibrils, radial pleated sheets and skin–core differentiation.[1] Energy absorption capacity of the composite depends both on the fibre and matrix properties and it is related to the failure mode of fibre, matrix (delamination and crashing) and cone formation.[2,3] Main challenge is cor-relating the penetration mechanisms to the governing variables of the problem: target and projectile charac-teristics (both geometrical and mechanical) and impact velocity. A review of impact processes carried out between 1978 and 1995 was presented by Corbett et al.[6] It was concluded that the type of failure occurring in metallic targets is primarily dependent on the projectile nose shape, since it has a significant influence on the energy absorption capability of the target.

The effect of the projectile characteristics o failure mode has been widely analysed on metals under high dynamic loading in order to describe the influence of different parameters: length mass, radius and nose shape.[7–10] However, few experimental and numerical models analyzing these effects are found for Kevlar® composite targets.

Modelling of high-speed impact of projectiles on Kevlar® targets requires the development of detailed composite models as well as the analysis of their associated response and failure mechanisms.[11]

Preliminary experimental and numerical study of Kevlar®-29 composite behaviour under high speed impact was carried out by Zhu et al.[2] and Van Hoof.[12] Zhu et al.[2] analysed the response of woven Kevlar®/polyester laminates of different thicknesses and lay-ups under quasi-static and dynamic penetration of cylindro-conical projectiles. Local deformation and fiber failure were found to be the main energy absorption mechanisms in impact perforation, moreover Kevlar® laminates exhibited better impact resistance to cylindro-conical projectiles when compared with aluminium. Van Hoof[12] performed ballistic impact tests on woven laminate Kevlar®-29 composite panels using different types of projectiles: two radius Fragment-Simulated Projectile (FSP) and conical projectiles (angle 120° and 37°). The relationship between the maximum backplane displacement and the impact energy was found to be nearly linear, at least within the range of impact energies considered in the work. This work was be used as a reference to calibrate the numerical model developed in this paper.

Silva et al.[13] reported experimental and numerical simulation of ballistic impact on Kevlar®-29/Vynilester laminates (2.4 mm of thickness) impacted with FSP. Numerical modelling was used to estimate the ballistic limit (V_{50}) and to simulate the failure modes and damage. Good correlation between computational simulations and experimental results was shown, in terms of both deformation and damage of the laminates.

Kumar et al.[14] simulated ballistic impact behaviour of Kevlar®/epoxy plate of 9.5 mm thickness using cylindrical-shaped flat-ended projectile of 6.15 g mass and 10 mm length and diameter projectile to study the influence of mass and diameter of the projectile on ballistic limit velocity. The study revealed that the ballistic limit velocity of the Kevlar/epoxy plate decreases with the increase in mass of the projectile when the diameter of the projectile is kept constant. When the diameter of the projectile increases the ballistic limit velocity for the Kevlar/ epoxy plate increases for constant mass.

Most studies available in the literature are restricted to few specific nose shapes, mainly flat, ogival, conical and spherical. However, it was demonstrated in previous works that a transition in the nose shapes (i.e., flat, ogive, hemispherical), has significant effect on the ballistic limit.[12] This fact supports the interest of studying the influence of the projectile geometry on ballistic behaviour of Kevlar® composites.

The objective of this work is developing a numerical analysis of the ballistic performances of Kevlar®-29 under impact of different double-nosed stepped cylindrical projectiles. Numerical modelling was carried out using the finite element code ABAQUS/EXPLICIT.[15] The aim was predicting the failure mode of the target as well as the ballistic limit. An analysis of the ballistic limit, failure mode and deformation of the targets due to impact of double-nosed projectiles is developed, discussed and compared with those involved in penetration of single-nosed flat and conical projectiles. A dimensional analysis relating perforation velocity, projectile properties, and armour system characteristics is presented.

Numerical modelling

The ballistic impact tests developed by van Hoof[12] and Wang et al.[16] have been used to validate the numerical model with the aim of analysing the influence of double-nosed stepped cylindrical projectiles on laminated woven Kevlar 29 composite.

The model was developed in the FE code ABAQUS/EXPLICIT using a Lagrangian approach, allowing efficient reproduction of the dynamic loading processes. Two solids are involved in the high velocity impact test, the projectile and the target based on Kevlar® composite. The projectiles were assumed to present a linear elastic behaviour ($E = 210$ GPa, $\nu = 0.3$). The behaviour of the Kevlar® composite was modelled through the introduction of a user subroutine VUMAT. The projectiles configuration was adapted from the work developed by Iqbal et al.[17] focused on metallic targets (1100-H14 aluminium alloy) in which their respective front and second nose shapes as conical-flat, flat–flat, conical–conical and flat-conical. Target thickness suitable for personal armour was selected. A mesh convergence study was performed, since the element size was found to have an effect on the numerical results.

The detailed description of the projectiles and the target, including modelling of the composite behaviour is given in the following sub-sections.

Projectile characteristics

As it was commented previously, the analysis of impact problems commonly involved the standard projectile shapes, mainly flat, conical, ogival and hemispherical. The analysis of these geometries has been focused on

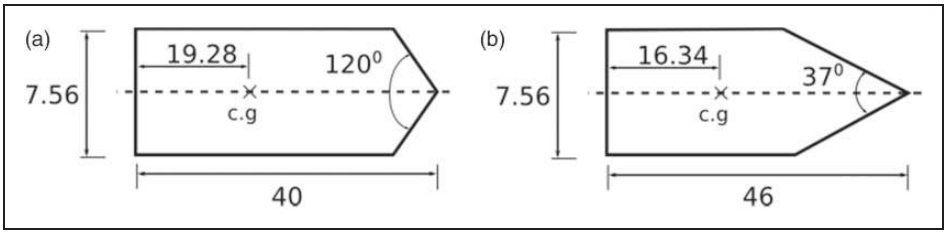

Figure 1. Schematic of the single-nosed projectiles ($m \approx 13.6g$) used by Ref. 12; (a) conical 120°; (b) conical 37°.

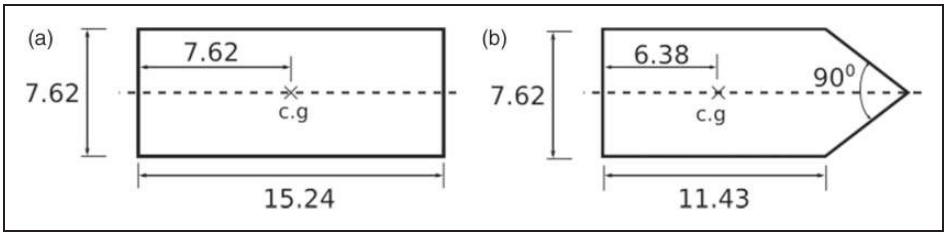

Figure 2. Schematic of the single-nosed projectiles ($m \approx 5g$) used by Ref. 16; (a) flat; (b) conical 90°.

metals[18–20] and also on composite materials.[2,10,14,21,22] In this work, the influence of the combination of conical and flat nose to obtain double-nose shape projectiles in the impact process is studied.

The projectiles defined in experimental tests used for validation[12,16] were made of 4340 steel and hardened to 30 HRc. The projectile was modelled as a 3D elastic deformable body since experimental and numerical tests revealed no plastic deformation on the projectile-surface after impact.[12,16] This definition allows reducing the computational time required for the simulations; the element type was C3D8R-linear brick element, with reduced integration (1 integration point)- in ABAQUS notation[15] with size 1.5 mm. The projectile behaviour was assumed to be elastic and a failure criterion was not required according to several works.[13,14] The mechanical properties are: Young Modulus $E = 210$ GPa and Poisson coefficient $\upsilon = 0.3$ as it was mentioned previously.

Two types of geometries were defined: single-nose shape projectiles and double-nose shape projectiles. The single-nose shape projectile was used for model validation. The numerical results obtained for this geometry were compared with the experimental data obtained in Ref. 12 focusing on conical projectiles with two nose angles ($\alpha = 120° - 37°$). The dimensions and mass of the conical projectiles are given in Figure 1. Another set of experimental data was used in order to complete the validation of the numerical model.[16] This study focused on the penetration of Kevlar®/epoxy target using a flat projectile and a conical projectile ($\alpha = 90°$). The dimensions and mass of these projectiles are given in Figure 2.

The double-nose shape projectiles defined in the present work had two cylindrical parts with the front part diameter equal to 3.81 mm and the back part diameter equal to 7.62 mm, see Figure 3. The mass of each projectile was 5 g and the diameter for both cylindrical zones was constant. In order to keep the mass and the diameters of the these projectiles identical, the total length of the projectiles was ranged (17.1, 19.61, 17.9, and 16.9 mm) for flat–flat, conical–conical, flat-conical and conical-flat projectiles, respectively. Therefore, these projectiles were comparable with single nose shape projectiles used in Ref. 16.

Composite target

Since the numerical model developed in this work has been validated using data from two different experimental works from the literature[12,16]; it was therefore necessary to develop two targets, each one with different geometry corresponding to the target used in the experiments. The target plates were meshed with C3D6 elements (6-node linear triangular prism) available in the ABAQUS code[15] with element size 0.75 mm.

The Kevlar®/epoxy plate corresponding to the experiments carried out in Ref. 12 was rectangular shaped, with dimensions $101{,}6 \times 152{,}4$ mm and thickness $h = 9{,}5$ mm, see Figure 4(a) . The impact tests carried out in Ref. 16 involved target plates with 100 mm diameter and two different thicknesses, 5 and 10 mm, respectively; see Figure 4(b).

The contact between the projectiles and the plates was defined with a penalty contact algorithm and a hard contact model according to ABAQUS code.[15] The "hard contact" option allows adjusting automatically the stiffness, generated by the "penalty contact

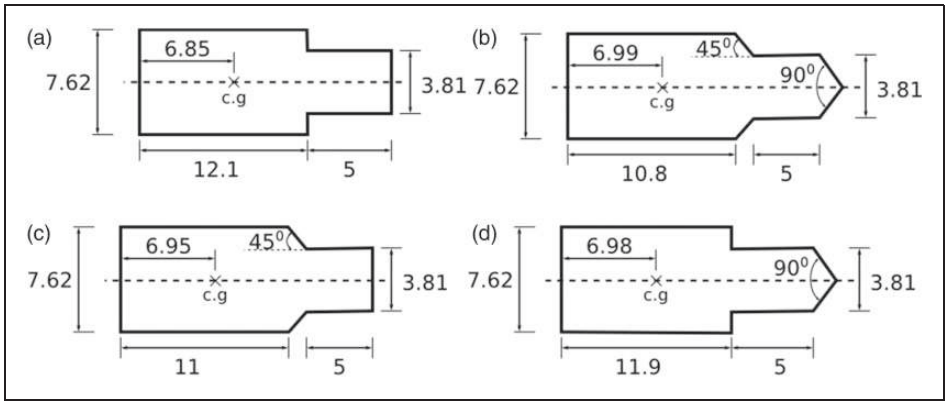

Figure 3. Schematic of the double-nosed projectiles ($m \approx 5g$): (a) flat–flat; (b) conical–conical; (c) flat-conical and (d) conical-flat.

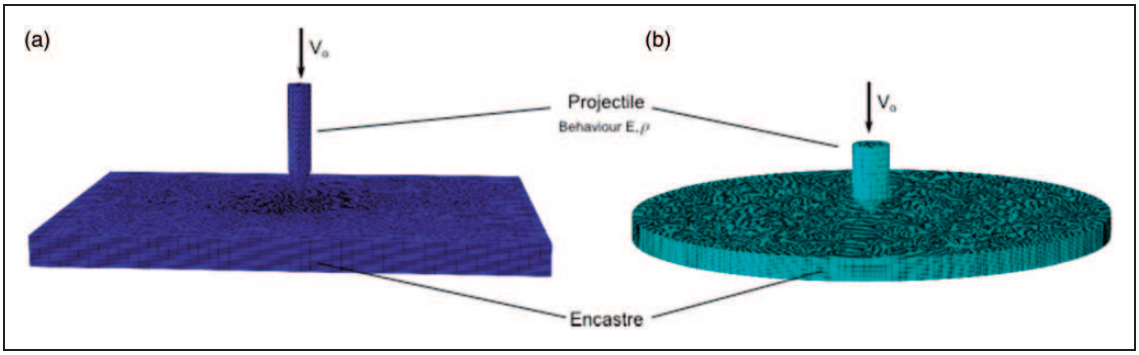

Figure 4. Three-dimensional model of projectiles and target plate. (a) Rectangular target plate[12] and (b) Circular target plate.[16]

algorithm," to minimize the penetration without affecting the time increment.

Concerning the friction it assumed a dynamic frictional coefficient μ equal to 0.1, according to Ref. 10 where it was concluded that the frictional effect was more prominent at low velocities, while it was diminished at higher velocities.

The mechanical behaviour of Kevlar® was modelled assuming elastic behaviour up to failure, the mechanical properties have been obtained from Ref. 12 and they are shown in Table 1. The values in this table are based on woven fabric Kevlar-29 (2×2 basket weave, 1500 denier) laminated using a polyvinyl butyral (PVB)-phenolic matrix (18% volume fraction). Kevlar-29 has a tenacity of 23.0 g/denier, an elongation to break of 3.6% and a modulus of 565 g/denier.[2,11,23]

Failure was predicted using a modification of the Hashin failure criteria[24] implemented in a VUMAT user subroutine, see Table 2. Numerous studies on low and high-velocity impact have demonstrated the accuracy of Hashin failure criteria to model the dynamic behaviour of carbon fibre composites, see for example Refs. 25–28. However, this set of failure criteria were developed for tape plies, thus the criteria were modified to consider the woven configuration of the Kevlar® plates analysed in this work. These modifications were implemented by Lopez-Puente et al.[26] in impact analysis.

Three equations were used to define the failure criteria: fibre failure was applied in directions 1 and 2 to predict the failure of warp and weft fibres, and delamination to consider the out-of-plane failure. The parameters in Table 3 are the following: σ_{11}, σ_{22}, and σ_{33}, are the stresses in longitudinal, transverse and through-the-thickness direction, respectively; σ_{12}, σ_{23}, and σ_{13}, are the shear stresses; X_{T1} and X_{T2} are the tensile strengths in warp and weft directions; Z_R is the tensile strength in the through-the-thickness direction; S_L is the longitudinal shear strength; S_T is the transverse shear strength. Failure occurs when any damage variable (d_{ij}) reaches the value 1.

Hashin formulation was implemented for the failure prediction of woven laminates through a VUMAT user subroutine, considering a three-dimensional stress state, including a procedure to degrade material properties. Under a given load, the stresses at each integration point were computed in the user subroutine. Then, each failure criterion was calculated as a function of stresses

Table 1. Mechanical properties of Kevlar®-29.

E_1 (GPa)	E_2 (GPa)	E_3 (GPa)	G_{12} (GPa)	G_{13} (GPa)	G_{23} (GPa)	ν_{12} (–)	ν_{13} (–)	ν_{23} (–)	ρ(kg/m^3)
18.5	18.5	6.0	0.77	5.43	5.43	0.25	0.33	0.33	1230

Table 2. Hou damage criteria: failure modes for fiber and matrix.

Failure mode	Hashin formulation
Fiber tension	$d_{1t}^2 = \left(\frac{\sigma_{11}}{X_{1T}}\right)^2 + \left(\frac{\sigma_{12}^2}{S_L^2}\right)$
	$d_{2t}^2 = \left(\frac{\sigma_{22}}{X_{2T}}\right)^2 + \left(\frac{\sigma_{12}^2}{S_L^2}\right)$
Delamination	$d_{mt}^2 = \left(\frac{\sigma_{33}}{Z_R}\right)^2 + \left(\frac{\sigma_{23}}{S_T}\right)^2 + \left(\frac{\sigma_{13}}{S_T}\right)^2$

and, if any failure mode was reached, the material properties at that point were degraded according to the failure mode. Fibre failure implies the degradation of all the mechanical properties, while delamination implies the degradation of stiffness in through-the-thickness direction. The verification of the in-plane tension failure criteria means that fibre rupture occurs and therefore the elements loss their resistance under in-plane loads but also under out-out-plane stresses. This procedure for properties degradation aims to reproduce physical observations associated to fibres breakage. These observations and consideration were demonstrated by Lopez-Puente et al.[26] and Ivañez et al.[29]

To avoid sudden changes in the stiffness of the finite elements when damage occurs leading to instability problems and lack of convergence during the simulation, the stress components were corrected using a smooth transition

$$\sigma_{ij} = \sigma_{ij} \bullet \quad 1 - \frac{2 - e^{s\left(D_i - \frac{1}{2}\right)}}{2 - e^{s/2}} \Bigg) \qquad (1)$$

where σ_{ij} and σ_{ij} are the stress before and after the correction, D_i is the corresponding damage parameter, and s is the variable which controls the slope of the stress decay when the damage is close to 1. The value $s = 30$ was adopted according to Ref. 26.

The reduction of elastic properties could lead to distorted elements involving numerical problems, thus the model required the use of an element erosion criterion. The stresses on a damaged element drop to values close to zero, while large deformations appear. These elements do not contribute to the strength or the stiffness of the plate, but they can cause lack of convergence during simulation and instability problems. Erosion criterion based on maximum strain criteria was implemented in the VUMAT subroutine to remove the distorted elements. After each time increment the longitudinal strains (ε_{11}, ε_{22} and ε_{33}) were evaluated, and the element was removed if one of the strains reached a critical value. The strains used in the erosion criterion were ($\varepsilon_{11}{}^{\max} = 1$, $\varepsilon_{22}{}^{\max} = 1$ and $\varepsilon_{33}{}^{\max} = 1$) high enough to prevent the deletion of elements that contribute to the stiffness and strength of the target. Thus, numerical problems were avoided and at the same time only strongly damaged elements were deleted. Since element deletion is controlled by the VUMAT user subroutine, distortion control was not used.

The parameters values for Hou model were obtained from the work of Gower et al.[30]

A mesh optimization of the target was carried out. The study of the influence of element has been developed with the model reproducing the experimental data given in Ref. 16 for two thicknesses: 5 mm and 10 mm.

In the case of the 5 mm thick target, the number of elements in the thickness was varied from 5 to 15. Figure 5(a) shows the residual velocity for the cases studied when initial impact velocity was 300 m/s. The time of simulation increased with the number of elements; however, the residual velocity converged to a constant value when the number of elements along the target thickness was equal or larger than 10. Thus the optimal configuration was defined with 10 elements through the target thickness.

The same observations were obtained in the case of thickness equal to 10 mm, the influence of the number of elements along the target thickness and the computational time is shown in Figure 5(b) when impact initial velocity was 300 m/s. The optimal configuration resulted in 20 elements through the target of 10 mm thickness.

Model validation

The numerical model was used to reproduce the experimental work developed in Refs. 12 and 16. Around 10–15 cases were simulated for a range of initial velocities of 200–700$\frac{m}{s}$ for each combination of projectile and target (around 90 simulations done in this section).

The experimental and calculated residual velocity corresponding to the experimental work in Ref. 16 is presented in Figure 6(a) and (b) showing good accuracy of the model predictions. When the conical projectile is used, the error between experimental and simulated

Table 3. Failure properties of Kevlar®-29.[23]

X_{1T} (MPa)	X_{2T} (MPa)	Z_R (MPa)	S_L (MPa)	S_T (MPa)	S_T (MPa)	Additional description
555	555	34.5	77	898	898	1. Modification of Hashin criteria to predict failure of woven laminates. 2. Mechanical properties degradation procedure. 3. Element deletion.

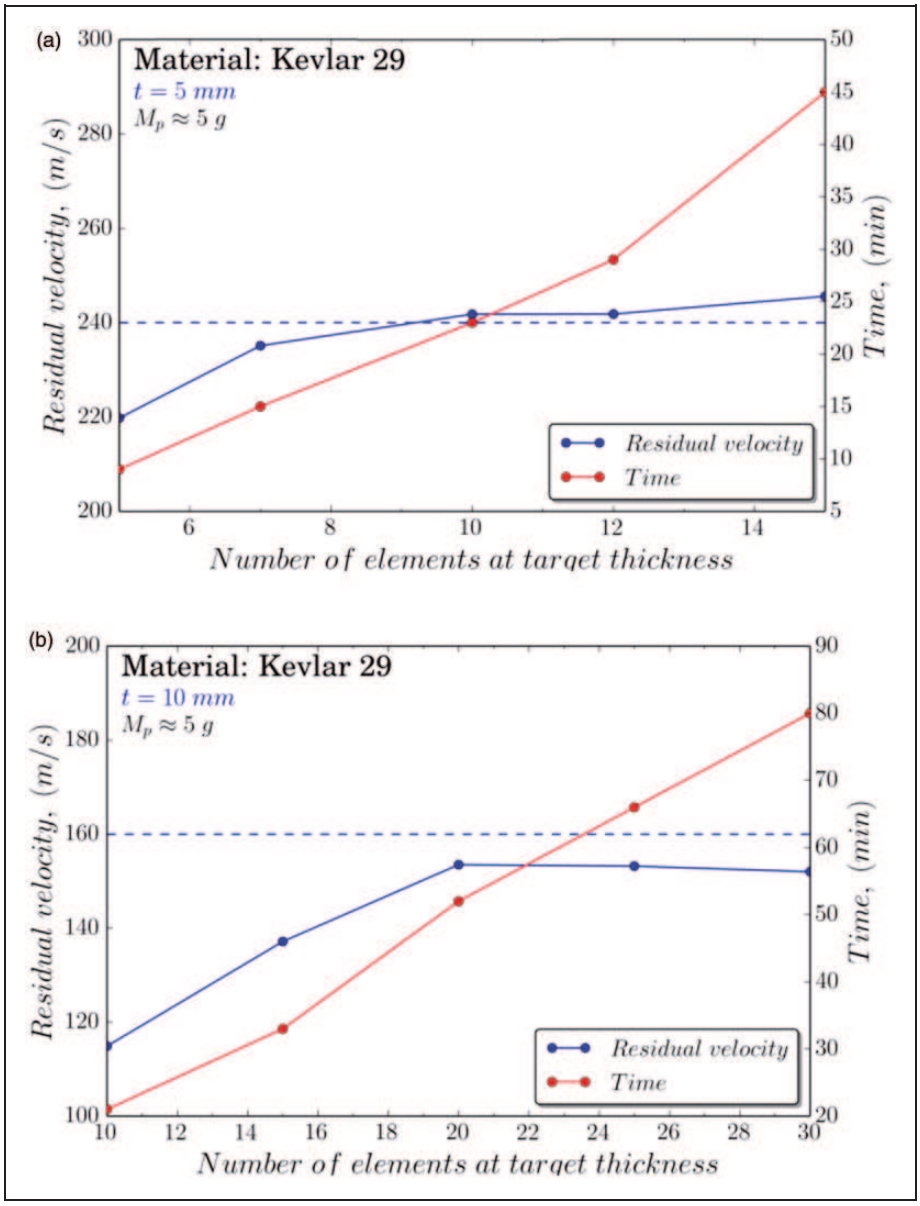

Figure 5. Mesh sensitivity analysis considering the element size in through thickness direction of target on residual velocity and computational time for two thickness: (a) 5 mm and (b) 10 mm. Initial impact velocity = 300 m/s.

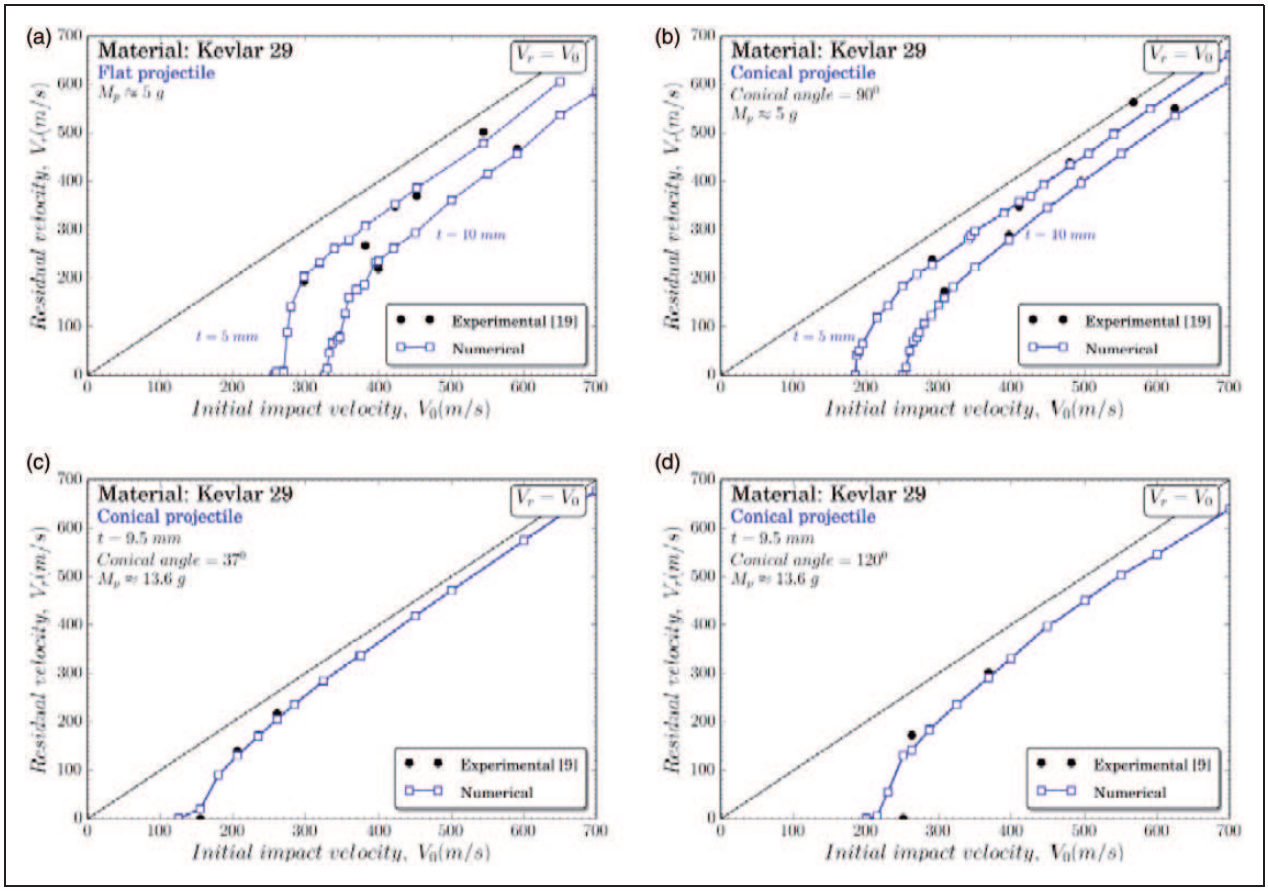

Figure 6. Comparison between experimental and predicted residual velocities for (a) Flat projectile,[16] (b) 90° conical projectile,[16] (c) 37° conical projectile[12] and (d) 120° conical projectile.[12]

residual velocities is 2.65% and 5.27% for targets with 5 and 10 mm thickness, respectively. This projectile also shows a very stable behavior for all the range of velocities studied. The error associated with the flat projectile is 4.45% and 3.34% for targets with 5 and 10 mm thickness, respectively. The behavior of this projectile differs from the predicted values especially for high velocities showing smaller penetration capacity. The average error for both projectiles is almost the same and it is always below 4%.

Figure 6(c) and (d) presents a comparison between the experimental and simulated residual velocities reproducing the test collected in Ref. 12. In this case, there are two conical projectiles and only one 9.5 mm thick target. The residual velocities predicted by the numerical model are very close to the experimental values, especially for the sharpest projectile since the error is 8.3%. The simulated ballistic limit for the 120° conical projectile is significantly below the experimental value due to the sudden fall of the residual velocity near the ballistic limit. Neglecting this point the error for the simulation is around 5%.

As the results obtained with the simulations are in good agreement with the experimental data used for validation, it was concluded that the numerical model accurately reproduces the real behavior of Kevlar®-29 being impacted by these projectiles.

Numerical investigation of the projectile shape effect

The models validated were used to analyse the performance of the Kevlar® target against different projectile configurations. The influence of the nose shape on residual velocity and damaged area was studied. Moreover, a dimensional analysis proposed in Ref. 31 was performed in order to relate the ballistic impact performance to fiber mechanical properties, regardless of impacting projectile mass, presented area or armor system areal density.

Residual velocity

Previous works dealing with impact in Weldox 460 E steel targets of Borvik et al.[18] and Iqbal et al.[17] showed

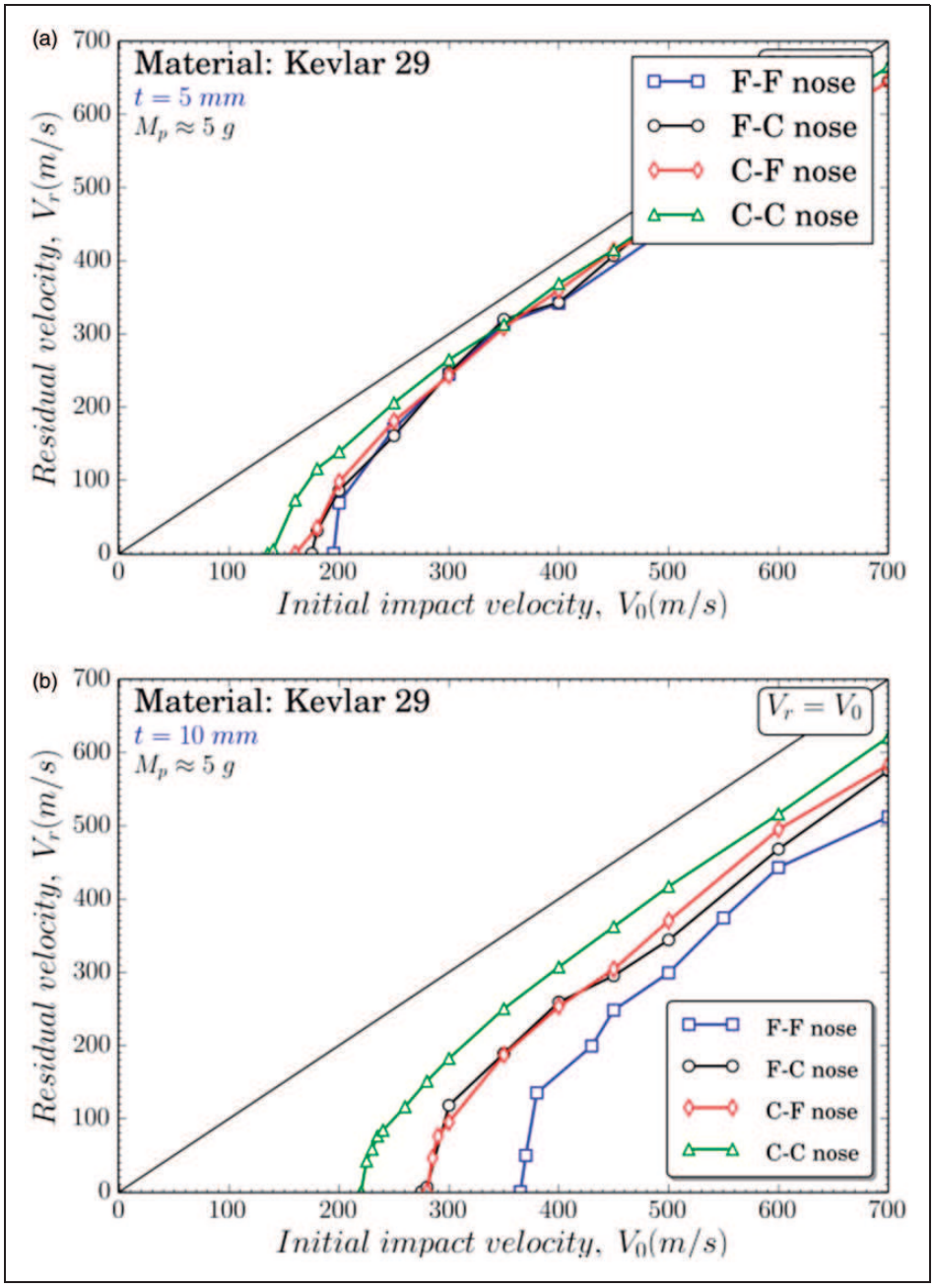

Figure 7. Predicted residual velocity curves for thickness plate of (a) 5 mm and 10 mm. Nomenclature of double-nose shape projectiles: flat–flat nose (F–F nose), flat-conical nose (F-C nose), conical-flat nose (C-F nose) and conical–conical nose (C–C nose).

the influence of the nose shape on the ballistic limit. According to these works, the ballistic limit was affected by the nose shape of the projectile observing that it is 62% higher for hemispherical and conical compared with flat nose. It is worth to note that the influence of the nose angle for conical projectiles is also important. The ballistic limit increases linearly with the decrease of the projectile nose angle. The smallest nose angle studied was 33.4° showing a ballistic limit 42% higher than flat nose projectiles, thus flat projectiles are more capable to penetrate metallic targets with moderate thickness.

Impact against circular target[16] (5 and 10 mm thick) was carried out considering only double-nose projectiles to study their ballistic limit and residual velocity after impact and the influence of the different nose shapes, using the model previously validated. The results are presented in Figure 7.

Figure 7(a) shows the residual velocity curve for the 5 mm thick target; it is possible to observe that the

projectiles present similar behaviour, especially for velocities over $360\frac{m}{s}$. The target offers the smallest resistance for the conical–conical projectile which has a slightly different behaviour, the difference is increased for velocities under 350 $\frac{m}{s}$, showing always the highest residual velocities of the study.

Figure 7(b) presents the residual velocity curve for the 10 mm thick target and in this case the differences are more accused for all impact velocities studied. In this case, the behaviour for the stepped shape-nose projectiles, conical-flat projectile and flat-conical projectile, is still similar, even both configurations presented the same ballistic limit velocity. The conical–conical projectile exhibits the maximum penetration and perforation capacity for all velocities studied since its residual velocity is always the highest, especially for impact initial velocities under $500\frac{m}{s}$. In addition, its behaviour is almost linear in the range studied.

The residual velocity curve for the conical–conical projectile always exceed the curve of the rest of configurations showing more penetration and perforation capacity. In addition, this projectile requires less energy to penetrate the target and this energy become constant for velocities greater than 400 $\frac{m}{s}$. On the other hand, the flat–flat projectile needs more energy to penetrate the target; because this projectile produces large plastic deformations in the target due to its geometry. Projectiles which impact firstly with a flat nose, show irregular behaviour between 300–400 $\frac{m}{s}$and 500–600 $\frac{m}{s}$ for the 5 mm and 10 mm thickness target, respectively. The non-linear behaviour is more evident for double-flat nose projectile.

Damaged area

Damaged area is defined as the area of the elements where the damage criterion is satisfied. It is measured through undistorted display of deleted elements (listed by the SDV6 user variable), using the software IMAGEJ which calculates the length of the pixels in the image and thus allows evaluating the area. The influence of the nose shape on the damaged area is shown in Figure 8. The evolution of damaged area with impact velocity was similar for all projectiles: the maximum damaged area was produced when impact velocity was equal to ballistic limit, and the extension of the damaged area decreased with impact velocity becoming more localized at highest velocities. Flat nose produced the maximum extension of the damaged area because the projectile cut the laminate through shearing action. On the other hand, conical–conical nose and conical nose led to the minimum damaged area because the projectile perforated the laminate with minimal delamination and tearing of the specimens. The damaged area produced by conical-flat nose was slightly higher than that produced by conical nose, the initial conical shape led to a perforation with minimal tearing of the target but the flat shape produced shear failure. These results agree with those found in the experimental results with flat-ended and conical projectiles reported by Tan and Khoo.[32]

Flat–flat and flat-conical noses produced different results depending on the target thickness. For the 5 mm thick specimens, the damaged area was similar to that produced by conical projectiles, but for 10 mm thick targets the damaged area was similar to that produced by flat noses. Due to the distances between the two noses, see Figure 3, thin laminates experienced the perforation of a flat nose with a small diameter and, after the first nose perforation, the damage was slightly increased due to the second nose. However, for the thicker laminates, both noses caused damage in the target and simultaneously the damaged area is increased.

Figure 9 shows the distribution of fibre failure criterion field for different projectile geometries when a 5 mm thick target is subjected to an impact velocity of approximately 250 m/s. The flat projectile produced the maximum damage extension because impact velocity was slightly lower than ballistic limit (Figure 9a); a great amount of energy was absorbed not only due to fibre failure but also due to delamination between adjacent plies. When the dominant failure mode was tearing induced by fibre failure at the back plies the damage was located around the impact area, see Figure 9(b) to (d). On the other hand, when the target failure was produced by shear stresses; Figure 9(e) and (f); the extension of fibre failure was enhanced leading to delamination between adjacent plies. This behaviour is similar to that observed in other dynamic shearing processes such as orthogonal cutting.[33]

Ballistic limit

The influence of the shape nose on the ballistic limit is showed in Figure 10 using projectiles with similar mass (5 g). In general, the ballistic limit for the 10 mm thick target was not found to be double to that presented by the 5 mm thick target.

It was also observed that the 5 mm thick target presented the highest ballistic limit against single-nosed flat projectile ($243m/s$) followed by the single- nosed conical projectile ($180\ m/s$). Furthermore, the lowest ballistic limit is achieved with conical–conical nosed projectile, $135\ m/s$. Thus, the conical–conical projectile is more efficient than the single-nosed flat projectile (40%). It was also noticed that the influence of conical-flat and flat-conical projectiles on ballistic limit was negligible. Regarding the perforation efficiency of double-nosed shape, the difference in ballistic limit

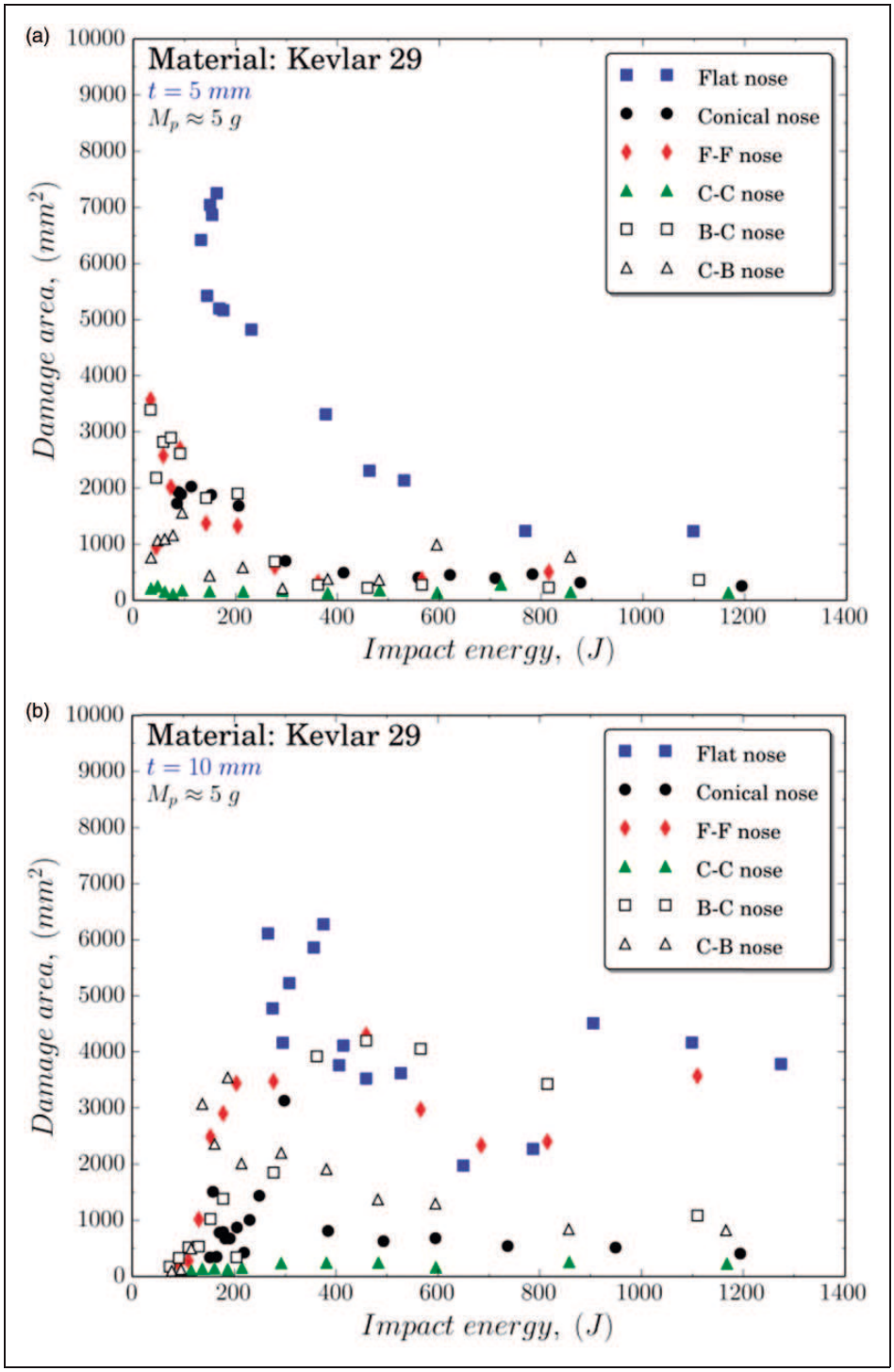

Figure 8. Extension of the damaged area vs. the impact energy for the different nose shape projectiles. Thickness of targets: (a) 5 mm and (b) 10 mm.

velocity between single-nosed flat projectile and double flat nose is less than 40%; however, this difference is higher in the case of conical nosed, around 45%.

On the other hand, the 10 mm thick target exhibited highest ballistic limit against flat–flat projectile (365 m/s) followed by single-nosed flat projectile (344 m/s), contrasting with the behaviour observed in the case of 5 mm thick target. The difference between the most efficient projectile (conical–conical projectile) and the lowest efficient projectile (flat–flat projectile) is similar to that presented by the 5 mm thick target, around 40%. The lowest ballistic limit was found for

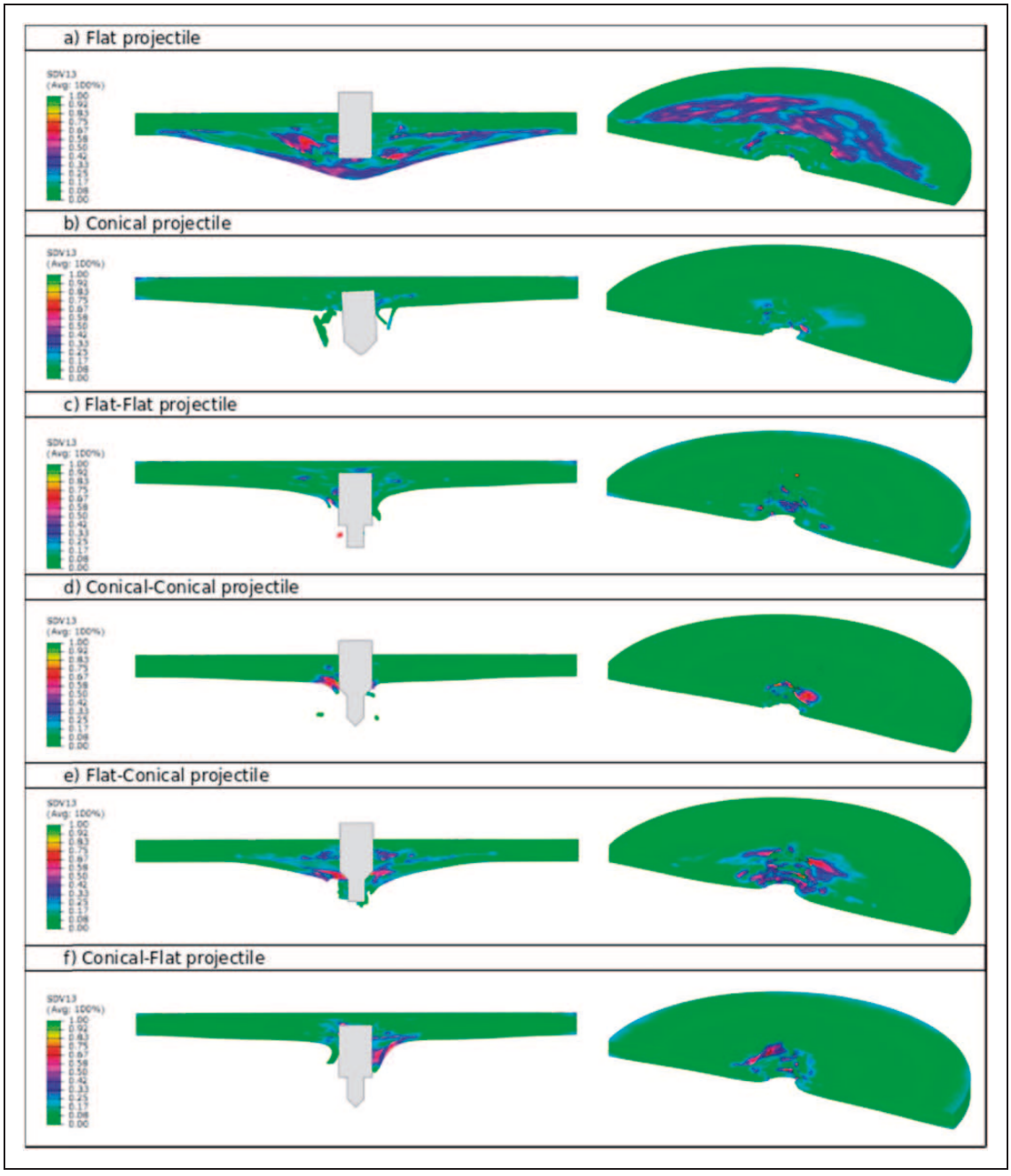

Figure 9. Distribution of fibre failure criterion under 5 mm of thickness and impact velocity of approximately 250 m/s for different nose-shape projectiles: (a) Flat projectile, (b) conical projectile, (c) flat–flat projectile, (d) conical–conical projectile, (e) flat-conical projectile and (f) conical-flat projectile.

conical–conical projectile ($220 m/s$) followed by the single-nosed conical projectile ($250 m/s$).

It can be concluded that the flat–flat projectile presented the lowest ballistic limit difference between the two thicknesses analysed. The conical–conical projectile is the most efficient perforating geometry when compared with other nose shape.

Moreover, a relevant observation can be drawn from this numerical analysis: the prediction of ballistic behaviour strongly depends not only on the projectile geometry but also on the target thickness.

A dimensionless methodology previously presented in Ref. 31 was developed. Cunniff[31] formulated a function in order to relate the normalized ballistic limit of a wide variety of fibre based armour systems to the target areal density ratio. This development allows relating ballistic impact performance to fibre mechanical properties independent of impacting projectile mass,

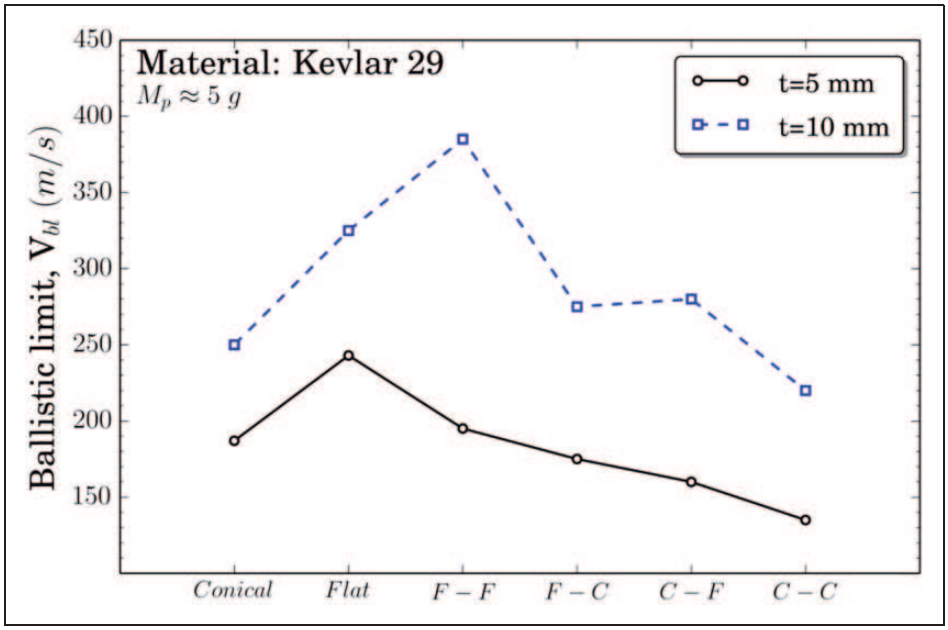

Figure 10. Ballistic limit V_{bl} versus projectile nose shape for both thicknesses tested.

presented area or armour areal density (weight per unit area) using following equation

$$\Phi\left(\frac{V_{bl}}{(U)^{\frac{1}{3}}}, \frac{A_d A_p}{m_p}\right) = 0 \tag{2}$$

where V_{bl} is the ballistic limit, A_p and A_d are the projectile presented area and the system areal density, respectively; $m_p$is the projectile mass and $U$is the product of fiber specific toughness and strain wave velocity, see equation (2)

$$U = \frac{\sigma\varepsilon}{2\rho}\sqrt{\frac{E}{\rho}} \tag{3}$$

The function Φ involves the incremental of the ballistic limit parameter$\left(\frac{V_{bl}}{(U)^{\frac{1}{3}}}\right)$ with the geometry ratio $\left(\frac{A_d A_p}{m_p}\right)$ showing a quasi-linear dependency according to Cunniff[31]

In order to obtain more information from this dimensionless analysis, new simulations were conducted for different thickness of the target ranging between 1 and 2.5 mm, the results are presented in Figure 11.

Relevant observations can be drawn from this analysis. It can be observed a growing trend of ballistic limit with geometry ratio $\left(\frac{A_d A_p}{m_p}\right)$ in the results. Thus, Figure 11 revealed that the relation between ballistic limit parameter$\left(\frac{V_{bl}}{(U)^{\frac{1}{3}}}\right)$ and the geometry ratio is almost linear. These observations agree with studies presented in Ref. 31.

For all values of geometry ratio, sharper projectile shapes resulted in lower ballistic limit than that presented by the flat projectiles, as it has been observed in numerous works.[6,10,18] Moreover, it is highlighted that the efficiency of single-nose conical projectile (120° angle nose) is similar to double-nose conical projectile (90° angle noses).

For high values of geometry ratio $\left(\frac{A_d A_p}{m_p}\right)$ and for the same nose angle, double-nose shape is the most efficient. It would therefore be necessary to take into account not only the nose angle but also the complete geometry of projectile in the design of protections of aramid fiber. In fact, ballistic limit varies around 14% between a single nose conical projectile (90° angle nose) and double-nose conical projectile (90° angle nose).

For low values of geometry ratio $\left(\frac{A_d A_p}{m_p}\right)$, the influence of nose angle in conical projectiles is negligible.

Conclusions

In this paper, a numerical analysis of the influence of projectile geometry on the ballistic performance of Kevlar® composite has been presented. A user subroutine reproducing the behaviour of Kevlar® has been implemented in the code ABAQUS/EXPLICIT. The model was validated comparing with experimental work in the literature showing good accuracy in the prediction of residual velocity and ballistic limit.

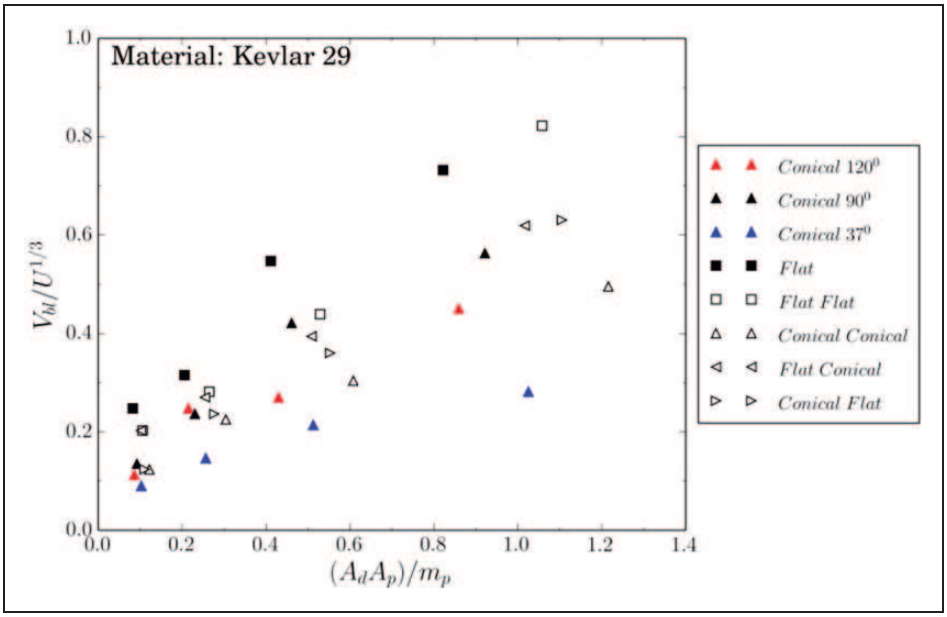

Figure 11. Ballistic limit ratio versus geometry configuration ratio.

The influence of the nose shape has been proved. The nose geometry of the projectile has lower influence on the ballistic limit velocity for thin targets. The influence of the projectile geometry increases with the target thickness.

Some conclusion can be drawn concerning the influence of the projectile geometry on ballistic performance of the target:

- The lowest ballistic limit was achieved by projectiles with conical–conical nose shape with low vertex angle and more weight for two different thickness of target. On the other hand, single-nosed flat projectiles was found to be less efficient (53%) to perforate thinner specimens (5 mm thick); however, double-flat nosed was found to be less efficient (68%) when penetrating thicker specimens (10 mm).
- The influence of double nosed shape was observed to be negligible for thinner targets. In other words, the use of conical-flat nosed projectile and flat-conical nosed required the same perforation energy. On the other hand, the influence of nose shape was important and it should be taken into account for high thicker laminates. This behavior is different to the experimental observations reported in the literature for metals, in this paper has been shown that conical single-nose was not always the most efficient penetrator.
- Main failure mechanism of the plates when impacted by conical projectiles was tearing produced by fiber failure leading to generation of local damage around the contact area. The opposite behavior was found when the targets are impacted by flat projectiles; in this case, the failure mechanism was shearing leading to a wide extension of damage due to delamination.

Declaration of Conflicting Interests

The author(s) declared no potential conflicts of interest with respect to the research, authorship, and/or publication of this article.

Funding

The author(s) disclosed receipt of the following financial support for the research, authorship, and/or publication of this article: The authors acknowledge the financial support for the work to the Ministry of Economy and Competitiveness of Spain under the Project RTC-2015-3887-8.

References

1. Pregoretti A and Traina M. In: Bunsell AR (ed.) *Handbook of tensile properties of textile and technical fibres*. Cambridge: Woodhead Publishing Limited, 2009, pp.354–436.
2. Zhu G, Goldsmith W and Dharan CKH. Penetration of laminated Kevlar® by projectiles – I. Experimental investigation. *Int J Solids Struct* 1992; 29: 399–420.
3. Sikarwar R, Velmurugan R and Madhu V. Experimental and analytical study of high velocity impact on Kevlar® Epoxy composite plates. *Cent Eur J Eng* 2012; 2: 638–649.
4. Zahid B and Chen X. Impact evaluation of Kevlar-based angle-interlock woven textile composite structures. *J Reinf Plast Comp* 2013; 32: 925–932.
5. Roy T and Chakraborty D. *Delamination in hybrid FRP laminates under low velocity impact*. *J Reinf Plast Comp* 2006; 25: 1939–1956.

6. Corbett GG, Reid SR and Johnson W. *Impact loading of plates and shells by free-flying projectiles: a review*. *Int J Impact Eng* 1996; 18: 141–230.
7. Montgomery TG, Grady PL and Tomasino C. The effects of projectile geometry on the performance of ballistic fabrics. *Text Res J* 1982; 52: 442–450.
8. Corran RSJ, Shadbolt PJ and Ruiz C. *Impact loading of plates: An experimental investigation*. *Int J Impact Eng* 1983; 1(1): 3–22.
9. Lim CT, Tan VBC and Cheong CH. *Perforation of high--strength double-ply fabric system by varying shaped projectiles*. *Int J Impact Eng* 2002; 27: 577–591.
10. Tan VBC, Lim C and Cheong C. *Perforation of high-strength fabric by projectiles of different geometry*. *Int J Impact Eng* 2003; 28: 207–222.
11. Naik NK, Shirirao P and Reddy BCK. Ballistic behaviour of woven fabric composites: formulation. *Int J Impact Eng* 2006; 32: 1521–1522.
12. Van Hoof J. *Modelling impact induced delamination in composite materials*. PhD Thesis, Carleton University, Ottawa, 1999.
13. Silva MAG, Cismaşiu C and Chiorean CG. Numerical simulation of ballistic impact on composite laminates. *Int J Impact Eng* 2005; 31: 289–306.
14. Kumar S, Singh I and Sharma A. Behavior of Kevlar®/ Epoxy composite plates under ballistic impact. *J Reinf Plast Comp* 2009; 29: 2048–2064.
15. Dassault Systèmes. Abaqus v6.12 Documentation – ABAQUS analysis user's manual. ABAQUS Inc; 6.12 2012.
16. Wang Y, Wang X, Hu X, et al. Experimental study on penetration and perforation of laminated Kevlar®. *J Beijing Inst Tech* 2004; 13: 317–323.
17. Iqbal MA, Khan SH, Ansari R, et al. Experimental and numerical studies of double-nosed projectile impact on aluminium plates. *Int J Impact Eng* 2013; 54: 232–245.
18. Børvik T, Langseth M, Hopperstad OSS, et al. Perforation of 12 mm thick steel plates by 20 mm diameter projectiles with flat, hemispherical and conical noses Part II: numerical simulations. *Int J Impact Eng* 2002; 27: 37–64.
19. Kpenyigba KM, Jankowiak T, Rusinek A, et al. Influence of projectile shape on dynamic behavior of steel sheet subjected to impact and perforation. *Thin-Walled Struct* 2013; 65: 93–104.
20. Rodríguez-Millán M, Vaz-Romero A, Rusinek A, et al. Experimental study on the perforation process of 5754-H111 and 6082-T6 aluminium plates subjected to normal impact by conical, hemispherical and blunt projectiles. *Exp Mech* 2014; 54: 729–742.
21. Nilakantan G, Wetzel ED, Bogetti TA, et al. Finite element analysis of projectile size and shape effects on the probabilistic penetration response of high strength fabrics. *Comp Struct* 2012; 94: 1846–1854.
22. Nilakantan G, Wetzel ED, Bogetti TA, et al. Deterministic finite element analysis of the effects of projectile characteristics on the impact response of fully clamped flexible woven fabrics. *Comp Struct* 2013; 95: 191–201.
23. Cheeseman BA and Bogetti BA. Ballistic impact into fabric and compliant composite laminates. *Comp Struct* 2003; 61: 161–173.
24. Hashin Z. Failure criteria for unidirectional fiber composites. *Trans ASME J Appl Mech* 1980; 47: 329–334.
25. Santiuste C, Sánchez-Sáez S and Barbero EA. Comparison of progressive-failure criteria in the prediction of the dynamic bending failure of composite laminated beams. *Comp Struct* 2010; 92: 2406–2414.
26. López-Puente J, Zaera R and Navarro C. Experimental and numerical analysis of normal and oblique ballistic impacts on thin carbon/epoxy woven laminates. *Compos Part A – Appl Sci* 2005; 39: 374–387.
27. Santiuste C, Barbero E and Miguélez MH. Computational analysis of temperature effect in composite bolted joints for aeronautical applications. *J Reinf Plast Comp* 2011; 30: 3–11.
28. Santiuste C, Díaz-Álvarez J, Soldani X, et al. Modelling thermal effects in machining of CFRP composites. *J Reinf Plast Comp* 2014; 33: 758–766.
29. Ivañez I, Santiuste C, Barbero E, et al. Numerical modelling of foam-cored sandwich plates under high-velocity impact. *Comp Struct* 2011; 93: 2392–2399.
30. Gower HL, Cronin DS and Plumtree A. Ballistic impact response of laminated composite panels. *Int J Impact Eng* 2008; 35: 1000–1008.
31. Cunniff PM. Dimensionless Parameters for optimization of textile-based body armor systems. In: *Proceedings of the 18th international and symposium on ballistics*, San Antonio, TX, 1999; 1303–1310.
32. Tan VBC and Khoo KJL. Perforation of Flexible Laminates by Projectile of Different Geometry. *Int J Impact Eng* 2005; 31: 793–810.
33. Santiuste C, Olmedo A, Soldani X, et al. Delamination prediction in orthogonal machining of carbon LFRP composites. *J Reinf Plast Comp* 2012; 31: 875–885.